crystals

MDPI

Article

Crystal Chemical Relations in the Shchurovskyite Family: Synthesis and Crystal Structures of $K_2Cu[Cu_3O]_2(PO_4)_4$ and $K_{2.35}Cu_{0.825}[Cu_3O]_2(PO_4)_4$

Ilya V. Kornyakov [1,2] and Sergey V. Krivovichev [1,3,*]

[1] Department of Crystallography, Institute of Earth Sciences, St. Petersburg State University, University Emb. 7/9, 199034 Saint-Petersburg, Russia; ikornyakov@mail.ru
[2] Laboratory of Nature-Inspired Technologies and Environmental Safety of the Arctic, Kola Science Centre, Russian Academy of Science, Fesmana 14, 184209 Apatity, Russia
[3] Nanomaterials Research Center, Federal Research Center–Kola Science Center, Russian Academy of Sciences, Fersmana Str. 14, 184209 Apatity, Russia
* Correspondence: s.krivovichev@kcs.ru

Abstract: Single crystals of two novel shchurovskyite-related compounds, $K_2Cu[Cu_3O]_2(PO_4)_4$ (**1**) and $K_{2.35}Cu_{0.825}[Cu_3O]_2(PO_4)_4$ (**2**), were synthesized by crystallization from gaseous phase and structurally characterized using single-crystal X-ray diffraction analysis. The crystal structures of both compounds are based upon similar Cu-based layers, formed by rods of the $[O_2Cu_6]$ dimers of oxocentered (OCu_4) tetrahedra. The topologies of the layers show both similarities and differences from the shchurovskyite-type layers. The layers are connected in different fashions via additional Cu atoms located in the interlayer, in contrast to shchurovskyite, where the layers are linked by Ca^{2+} cations. The structures of the shchurovskyite family are characterized using information-based structural complexity measures, which demonstrate that the crystal structure of **1** is the simplest one, whereas that of **2** is the most complex in the family.

Keywords: shchurovskyite; synthesis; X-ray diffraction; crystal structure; oxocentered tetrahedra

Citation: Kornyakov, I.V.; Krivovichev, S.V. Crystal Chemical Relations in the Shchurovskyite Family: Synthesis and Crystal Structures of $K_2Cu[Cu_3O]_2(PO_4)_4$ and $K_{2.35}Cu_{0.825}[Cu_3O]_2(PO_4)_4$. *Crystals* **2021**, *11*, 807. https://doi.org/10.3390/cryst11070807

Academic Editor: Francesco Capitelli

Received: 28 June 2021
Accepted: 9 July 2021
Published: 11 July 2021

1. Introduction

The last two decades are marked by the increased interest in mineralogical data from the field of material sciences. Since the discovery of a quantum spin liquid state in herbertsmithite [1,2], the number of mineralogically inspired studies in this field has grown exponentially: from the investigation of magnetic properties of the atacamite-group minerals [3–7], to other Cu minerals such as lindgrenite [8], libethenite [9], dioptase [10,11], volborthite [12], vesigneite [13,14], etc. [15–17]. The most important common feature of all these mineral structures is the presence of Cu^{2+} cations in variable coordination geometries, a consequence of the Jahn–Teller effect [18–20] that results in the existence of at least four most common coordination geometries [21–23] with a diversity of transitional forms. Such a flexibility of Cu^{2+}-centered coordination polyhedra leads to the occurrence of a multitude of structure types with interesting physical properties tunable through an interplay between structure and chemical composition.

A number of mineral-related structures are characterized by the presence of 'additional' oxygen atoms that do not participate in the formation of strongly bonded "acid residue" complexes (sulfate, vanadate, phosphate, arsenate, selenite groups, etc.). These structures can be described in terms of anion-centered tetrahedra and attract special attention due to their magnetic properties controlled by the local structure of oxygen-based copper polycations [24–26]. For example, magnetic studies were performed for such anion-centered-based minerals as ilinskite [27], averievite [28,29], yaroshevskite [30], atlasovite [31], etc.

An important trend in the study of magnetic phases is the synthesis of novel mineral-inspired compounds, revealing the dynamics of structural changes and crystal chemical relations in various mineral groups. Recently, we discovered new structure types in the averievite family, $(MX)Cu_5O_2(TO_4)_2$ (T^{5+} = P, V; M^+ = K, Rb, Cs, Cu; X = Cl, Br) [32], which demonstrate significant changes in the first coordination spheres of Cu^{2+} cations with the changes induced by the size of alkali metal ions, resulting in significant geometrical changes within the kagomé arrangements of magnetic Cu^{2+} centers.

Aksenov et al. [33] reported on the synthesis and magnetic properties of $Rb_2CaCu_6(PO_4)_4O_2$, belonging to the shchurovskyite family, originally discovered by Pekov et al. [34] in the fumaroles of the Great fissure Tolbachik eruption, Kamchatka peninsula, Russia. Herein, we report on the synthesis and crystal structures of two novel compounds of the shchurovskyite family. Despite the fact that both structures significantly differ from the original shchurovskyite structure, both of them possess shchurovskyite-type Cu-based layers.

2. Materials and Methods

2.1. Synthesis

Single crystals of **1** ($K_2Cu[Cu_3O]_2(PO_4)_4$) and **2** ($K_{2.35}Cu_{0.825}[Cu_3O]_2(PO_4)_4$) were prepared via gas phase crystallization, successfully employed for the simulation of fumarolic mineral formation in a number of previous experiments [30,35,36]. Stoichiometric amounts of copper oxide (CuO, 99%, Vekton, St. Petersburg, Russia), copper pyrophosphate ($Cu_2P_2O_7$, 99%, Vekton) and potassium chloride (KCl, 99%, Vekton) taken in the 6:2:3 molar ratio were ground in an agate mortar. Due to the hygroscopic nature of potassium chloride [37,38], the resulting mixture was loaded into a porcelain boat and annealed at 250 °C for ~24 h in air. The mixture was further loaded into a fused silica ampule, evacuated to 10^{-2} mbar, sealed and placed horizontally in a furnace and heated to 800 °C over a period of 6 h. After two days, the furnace was cooled to 350 °C over a period of 72 h and switched off. The resulting sample contained single crystals of $K_2Cu[Cu_3O]_2(PO_4)_4$ (**1**), $K_{2.35}Cu_{0.825}[Cu_3O]_2(PO_4)_4$ (**2**), $Cu_5O_2(PO_4)_2$ [39] and copper oxide. All the compounds were found in a source zone of the ampule.

2.2. Single-Crystal X-ray Diffraction Study

Single crystals of both compounds were selected for data collection under an optical microscope, coated in an oil-based cryoprotectant and mounted on cryoloops. Diffraction data for **1** were collected using a Bruker APEX II DUO X-ray diffractometer (Bruker Co., Billerica, MA, U.S.A.) operated with a monochromated microfocus MoKα tube (λ = 0.71073 Å) at 50 kV and 0.6 mA and equipped with a CCD APEX II detector. Diffraction data for **2** were collected using a Rigaku XtaLAB Synergy S X-ray diffractometer (Rigaku Co., Tokyo, Japan) operated with a monochromated microfocus MoKα tube (λ = 0.71073 Å) at 50 kV and 1.0 mA and equipped with a CCD HyPix 6000 detector. Exposures were 10 and 74 s per frame for **1** and **2**, respectively. CrysAlisPro software [40] was used for the integration and correction of diffraction data for polarization, background and Lorentz effects as well as for an empirical absorption correction based on spherical harmonics implemented in the SCALE3 ABSPACK algorithm. The unit cell parameters (Table 1) were refined using the least-squares technique. The structures were solved by a dual-space algorithm and refined using the SHELX programs [41,42] incorporated in the OLEX2 program package [43]. The final models include coordinates and anisotropic displacement parameters (Tables A1 and A2).

Table 1. Crystallographic data and refinement parameters for **1** and **2**.

Compound	**1**	**2**
Formula	$K_2Cu[Cu_3O]_2(PO_4)_4$	$K_{2.35}Cu_{0.825}[Cu_3O]_2(PO_4)_4$
Space Group	*P*-1	$P2_1/n$
a, Å	5.7787(3)	16.7138(4)
b, Å	8.2612(4)	11.2973(3)
c, Å	8.3717(4)	16.8031(4)
α, °	95.813(4)	90
β, °	103.239(4)	90.775(2)
γ, °	96.821(4)	90
V, Å^3	382.85(3)	3172.47(13)
μ, mm^{-1}	10.601	10.137
Z	1	8
D_{calc}, g/cm^3	4.055	3.925
Color	Light green	Intense green
Total reflections	4126	37428
Unique reflections	1759	7219
Reflection with $\|F_o\| \geq 4\sigma_F$	1491	5761
Angle range 2θ, °, MoKα	5.01 to 54.998	6.492 to 55
R_{int}, R_σ	0.0286, 0.0359	0.0368, 0.0303
R_1, wR_2 ($\|F_o\| \geq 4\sigma_F$)	0.0285, 0.0602	0.0394, 0.0847
R_1, wR_2 (all data)	0.0368, 0.0634	0.0535, 0.0901
GOOF	1.078	1.032
ρ_{min}, ρ_{max}, e/Å^3	0.69 / −0.64	1.57 / −1.94
CSD	2092265	2092266

3. Results

Crystal Structure Descriptions

The crystal structure of **1** contains four symmetrically distinct Cu^{2+} cations, three of which (Cu1, Cu2 and Cu3) form the shchurovskyite-type layer as shown in Figure 1a. Considered in terms of the cation-centered polyhedral, the basic unit of the structure is a rod of edge-sharing $Cu3O_5$ square pyramids (Cu3 · · · Cu3 = 2.856 Å), extended along [100]. The orientation of apical vertices (O_{ap}) of square pyramids alternates up (**U**) and down (**D**) relative to the (010) plane, giving the **UDUDUD** sequence within the rod, with the Cu–O_{ap} bond distance equal to 2.239 Å (Figure 1c). Each rod is decorated by $Cu1O_6$ octahedra and $Cu2O_5$ triangular bipyramids from both sides in the (010) plane. The $Cu1O_6$ octahedron shows a typical [4+2] distortion with four short (1.887–2.097 Å) and two long (2.706 and 2.768 Å) Cu–O bonds. It is noteworthy that the Cu1 site has one more elongated (2.936 Å) Cu–O distance to the O atom located near one of the apical ligands (O · · · O = 2.500 Å), which corresponds to the edge of the $(PO_4)^{3-}$ tetrahedron. Such a coordination geometry of Cu^{2+} cations is rather rare and, as far as we know, among all the natural Cu^{2+}-containing oxysalts, it was observed in the crystal structures of cesiodymite, cryptochalcite and saranchinaite, which are the products of fumarolic activity of the Tolbachik volcano [44,45]. The $Cu1O_6$ octahedron shares a common edge with the $Cu2O_5$ triangular bipyramid. The equatorial plane of the $Cu2O_5$ bipyramid is formed by one short (1.944 Å) and two elongated (2.237 and 2.299 Å) Cu-O bonds. The apical Cu2–O_{ap} bond lengths are equal to 1.884 and 1.920 Å. The $Cu2O_5$ bipyramid is slightly distorted due to the Berry twist mechanism [46,47]: the O_{ap}–Cu2–O_{ap} and O_{eq}–Cu2–O_{eq} angles are equal to 166.6 and 124.4°, respectively.

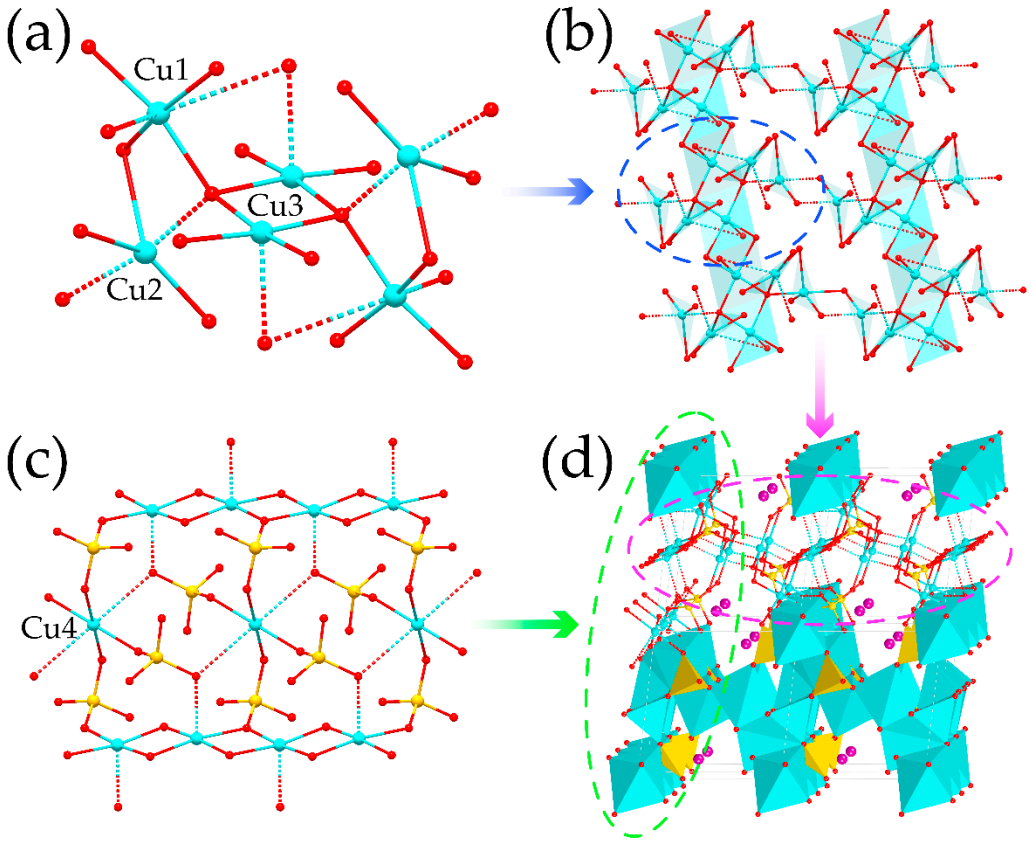

Figure 1. The key features of the crystal structure of **1**: (**a**) the linkage of coordination polyhedra of the Cu1, Cu2 and Cu3 atoms; (**b**) the Cu-based layer; (**c**) the rods of $Cu3O_5$ square pyramids and $Cu4O_6$ octahedra, connecting the Cu-based layers; (**d**) lateral view of the crystal structure. Legend: Cu = cyan, O = red, P = yellow, K = purple.

The rods are linked into the Cu-based polyhedral layer parallel to (010) due to the edge-sharing of two adjacent $Cu2O_5$ triangular bipyramids belonging to the neighboring rods (Figure 1b). The connection between the layers in the shchurovskyite-related compounds proceeds via the PO_4 tetrahedra. In the crystal structure of **1**, each $P2O_4$ tetrahedron shares common vertices with the $Cu3O_5$ square pyramid and $Cu2O_5$ triangular bipyramid of one layer, and with the $Cu1O_6$ octahedron of the adjacent layer. In opposition, the $P1O_4$ tetrahedron is located within the layer, and shares common vertices with two $Cu2O_5$ triangular bipyramids and one $Cu1O_5$ square pyramid. There is one additional Cu4 site located in between the layers (Figure 1c) and coordinated by six oxygen atoms, belonging to the PO_4 tetrahedra, to form [4+2]-distorted octahedron with four short (1.977 (×2) and 1.984 (×2) Å) and two long (2.823 (×2) Å) Cu4-O bonds. Two opposite vertices of the equatorial plane of the $Cu4O_6$ octahedron are common with two $Cu3O_5$ square pyramids of adjacent Cu-based layers. The resulting framework has channels filled by K^+ cations (Figure 1d). There is one symmetrically distinct K atom, coordinated by six oxygen atoms (2.633–2.959 Å), with the <K1 · · · K1> distance equal to 3.865 (3) and 3.732 (3) Å. The calculation of the effective width (e.c.w.) of the channels, by subtracting the ionic diameter of O^{2-} (2.7 Å) from the shortest and longest O · · · O distances across the channel [48], shows that the channel in the structure of **1** is much smaller than in the structure of shchurovskyite: 1.3 × 4.6 $Å^2$ in **1** versus 2.8 × 5.9 $Å^2$ in shchurovskyite.

As with all known shchurovskyite-type minerals and compounds, the crystal structure of **1** contains so-called 'additional' oxygen atoms (O_{add}), allowing it to be described in terms of anion-centered tetrahedra [24,25]. The structure of **1** contains one symmetrically distinct 'additional' oxygen atom tetrahedrally coordinated by two Cu3, one Cu1 and one Cu2 atoms (Figure 1a). The O_{add}–Cu bond lengths are the shortest among all Cu–O bonds

and span the range of 1.881–1.913 Å. Two OCu_4 tetrahedra share a common Cu3 · · ·Cu3 edge to form a $[O_2Cu_6]^{8+}$ dimer.

The crystal structure description of **2** is far more difficult to describe due to its disordered nature and the enlarged unit cell, which is a consequence of the increased number of symmetrically distinct positions of all atoms. There are two symmetrically distinct rods of CuO_5 square pyramids in **2**. The first rod consists of the $Cu3O_5$ and $Cu4O_5$ pyramids, alternating along [010], whereas the alternation of the $Cu8O_5$ and $Cu9O_5$ pyramids builds the second rod (Figure 2a,c,e). The equatorial Cu–O_{eq} bond lengths within square pyramids are in the range of 1.898–1.966 Å. The apical oxygen atom of the $Cu8O_5$ square pyramid is split into two positions, resulting in the Cu8-O_{ap} bond lengths of 2.579 and 2.739 Å; the apical bond lengths in the other square pyramids vary from 2.386 to 2.469 Å. The apical vertices of the square pyramids within the rods are oriented according to the **UUDDUU** sequence, which is different from the sequence **UDUD** observed in **1**.

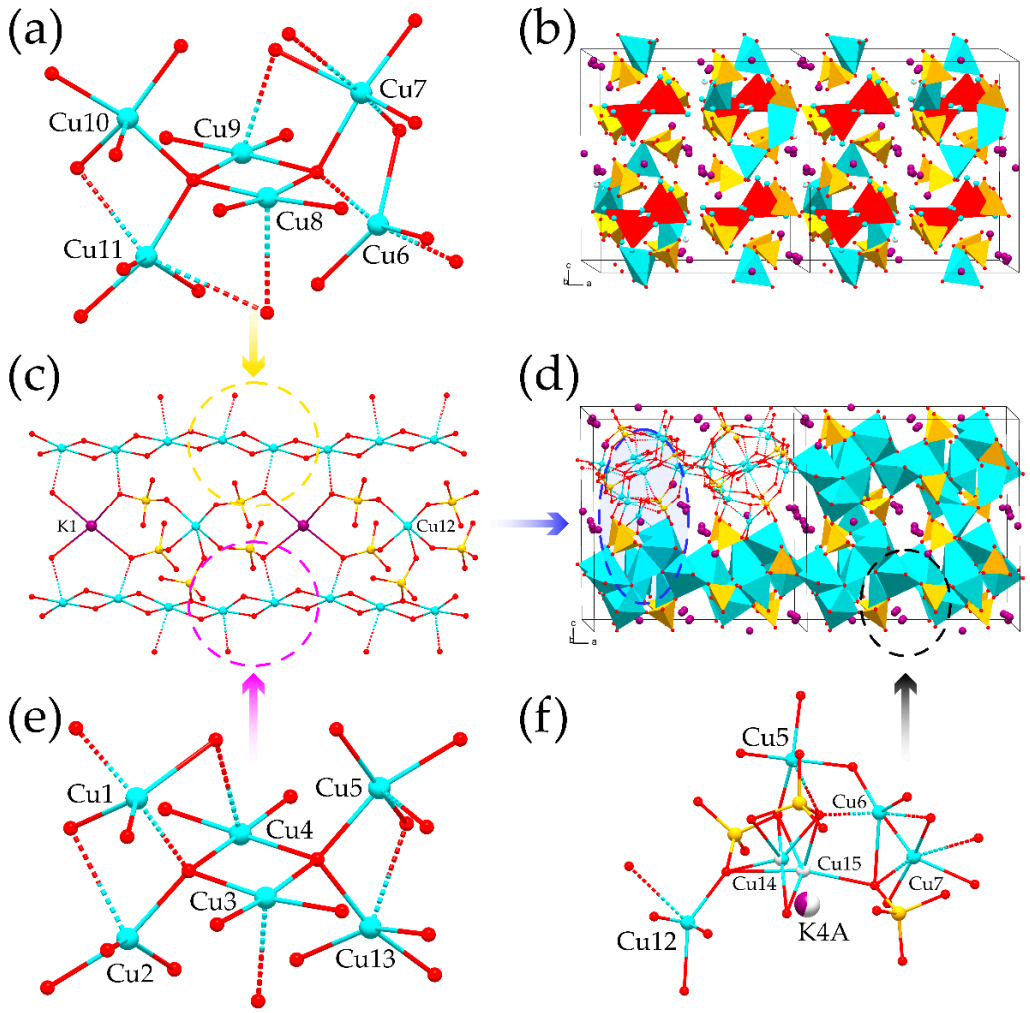

Figure 2. The key features of the crystal structure of **2**: (**a**) the fragment of the Cu9···Cu8 rod; (**b**) the arrangement of anion-centered tetrahedra (shown in red); (**c**) two symmetrically distinct rods linked via the $Cu12O_6$ octahedra; (**d**) lateral view of the crystal structure; (**e**) the fragment of the Cu3···Cu4 rod; (**f**) the disordered arrangement of the Cu14 and Cu15 sites, and associated K4A site. Disordered oxygen atoms are shown at most probable positions. Legend: as in Figure 1.

The local coordination of the Cu atoms, involved in the orthogonal connection of the polyhedral rods, is different from those observed in the crystal structure of **1**: instead of one symmetrically distinct Cu^{2+}-centered triangular bipyramid, there are four distinct Cu^{2+} polyhedra, forming two types of bridges. The bridge of the first type is formed by

the dimer of edge-sharing $Cu2O_5$ and $Cu10O_5$ square pyramids. The average <Cu–O_{eq}> bond distances are equal to 1.953 and 1.966 Å for the $Cu2O_5$ and $Cu10O_5$ pyramids, respectively, whereas the apical bond lengths are 2.597 and 2.305 Å, respectively. Note that the $Cu2O_5$ square pyramid can be considered as a [4+1+1]-distorted octahedron due to the presence of an additional elongated Cu–O_{ap} bond equal to 2.939 Å. The bridge of the second type consists of the $Cu5O_5$ square pyramid and $Cu6O_5$ triangular bipyramid, sharing a common edge. The $Cu5O_5$ square pyramid is similar to the $Cu2O_5$ and $Cu10O_5$ pyramids, with the average <Cu5–O_{eq}> bond length equal to 1.947 Å and the Cu–O_{ap} bond of 2.528 (6) Å. The triangular–bipyramidal coordination geometry of the Cu6 atom is similar to that in **1**, with one short and two elongated (1.88, 2.305 and 2.188 Å) equatorial bonds, and two short (1.965 and 1.880 Å) apical bonds. Taking the crystal structure of **1** as an archetype, the $Cu1O_6$ octahedron in **1** is replaced in **2** by four symmetrically distinct Cu atoms, attached to the rods. The $Cu7O_6$ and $Cu11O_6$ octahedra share common vertices with the $Cu8O_5$ and $Cu9O_5$ square pyramids of the rods (Figure 2a). While the $Cu7O_6$ octahedron shows a typical [4+2]-distortion, the coordination geometry of the Cu11 atom is difficult to assess due to the disorder of one equatorial and one apical ligands. We suppose the overlap of two possible coordination geometries—octahedral and triangular–bipyramidal. The presence of one or another geometry depends on the rotation of the $P5O_4$ tetrahedron that has three split oxygen positions with the site-occupancy factors (S.O.F.) equal to 0.663:0.337. Equatorial bond lengths of the $Cu11O_5$ triangular bipyramid are equal to 1.93, 2.212 and 2.474 Å, whereas the apical bonds are 1.905 and 1.912 Å long. The octahedral coordination geometry of the Cu11 atom shows the [3+1+2]-distortion, with three short (1.905–2.051 Å) and one elongated (2.212 Å) equatorial bonds and two long apical bonds (2.474 and 2.809 Å). The second rod is decorated by the the $Cu13O_6$ octahedra and $Cu1O_5$ triangular bipyramids (Figure 2e). The $Cu13O_6$ octahedron is [4+1+1]-distorted with four short equatorial (1.897–2.052 Å) and two long apical bonds (2.476 and 2.897 Å). The bond distribution in the $Cu1O_5$ polyhedron is different from those in other triangular bipyramids in **1** and **2**: there are two apical bonds (1.906 and 1.911 Å) slightly shorter than the equatorial bonds (2.070–2.172 Å).

The Cu^{2+}-centered polyhedra in **2** form the Cu-based layer parallel to the (001) plane. The comparison with the structure of **1** reveals the significant difference between two structures: instead of the CuO_6 octahedra connecting the layers in **1**, the crystal structure of **2** shows an alternation of the Cu and K atoms along [010] (Figure 3c). There are two symmetrically distinct fully occupied Cu12 and K1 sites. The Cu12 site is coordinated by five oxygen atoms to form a [4+1]-distorted square pyramid. Taking into account that positions of two neighboring oxygens in the equatorial plane of the $Cu12O_5$ polyhedron are disordered, the average < Cu12–O_{eq}> bond length is 1.972 Å. The coordination geometry of the Cu12 site can also be considered as transitional from square-pyramidal to square-planar due to the long Cu12–O_{ap} bond length (2.731 Å). The K1 atoms are coordinated by eight oxygen atoms of the phosphate groups, with five relatively short (2.711–2.857 Å) and three long (3.375–3.318 Å) K1–O bonds.

The enlargement of the unit cell results in the presence of the second symmetrically distinct intra-framework channel. Both types of channels are filled by highly disordered K atoms (Figure 2d). The first channel contains K2 and K3 atoms, each split into two and three symmetrically distinct partially occupied positions, respectively. The displacement of the K atoms, placed in average positions, is similar to that observed in the structure of **1** due to the zigzag arrangement within the channel, with the $K2_{av}\cdots K3_{av}$ and $K3_{av}\cdots K3_{av}$ distances equal to 3.992 and 4.124 Å, respectively. The effective channel width (1.3 × 5.8 $Å^2$) is close to that observed in the crystal structure of shchurovskyite [34]. The content of the second symmetrically distinct channel is significantly different from that observed in any other shchurovskyite-type structures. Herein, along with the disordered K atoms, additional Cu atoms are present. The Cu site within the channel is split into two symmetrically distinct positions, Cu14 and Cu145, with S.O.F. of 0.5 and 0.15, respectively (Figure 3f). While the most occupied Cu14 position exhibits a typical square-pyramidal coordination geometry

(2.012–2.735 Å), the Cu15 site shows a different bond distribution, having one short (2.033 Å) and four elongated (2.212–2.490 Å) bonds, a consequence of the low occupancy of the disordered configuration. The K atoms are concentrated near to the center of the channel with the K–O bond lengths in the range of 2.564–3.40 Å. Due to the presence of the additional Cu atoms, the effective width of channels is reduced to 1.5 × 3.0 $Å^2$.

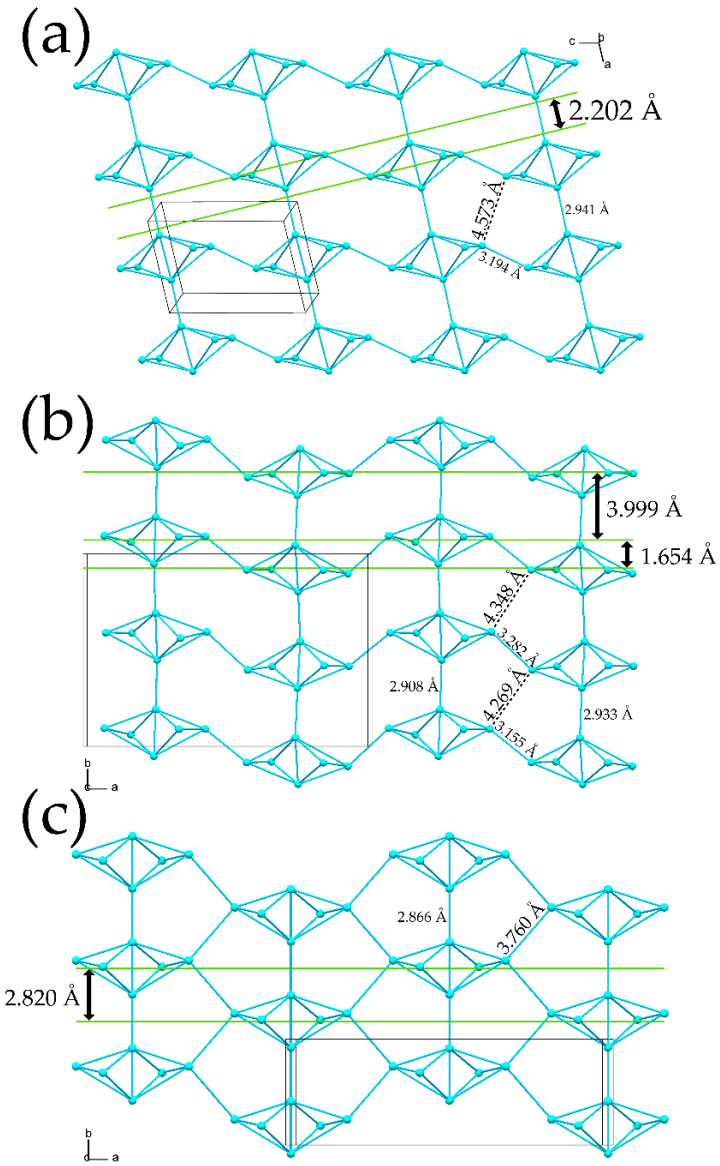

Figure 3. Cu-based layers in the crystal structures of **1** (**a**), **2** (**b**) and $Rb_2Ca[Cu_3O]_2(PO_4)_4$ (**c**). Thin black lines show boundaries of unit cells. Legend: as in Figure 1. See details in the text.

The crystal structure of **2** contains four symmetrically distinct 'additional' oxygen atoms, tetrahedrally coordinated by copper atoms, with the O_{add}–Cu bond lengths varying from 1.881 to 1.928 Å (Figure 2b).

4. Discussion

The crystal structures of shchurovskyite, $K_2Ca[Cu_3O]_2(AsO_4)_4$, dmisokolovite, $K_3[Cu_5AlO_2](AsO_4)_4$, and synthetic $Rb_2Ca[Cu_3O]_2(PO_4)_4$ are based upon Cu-based oxo-layers, linked via $(PO_4)^{3-}$ tetrahedra [33,34]. The hetero-polyhedral framework contains channels, filled by K^+ cations, and one additional position between the copper layers, occupied by Ca^{2+} and K^+ atoms in shchurovskyite and dmisokolovite, respectively. Unlike

the structure of both minerals, these additional positions in the crystal structures of **1** and **2** are occupied by Cu^{2+} cations, connecting the Cu-based layers, which results in the formation of a Cu-based porous framework, decorated by $(PO_4)^{3-}$ tetrahedra and containing potassium atoms within the channels.

As was mentioned above, all the shchurovskyite-type structures can be described as consisting of Cu-based layers. The simplest way to distinguish the main features of each structure is a topological analysis, which can be performed by means of representation of the connectivity of copper atoms in terms of nets. In order to reduce the influence of chemical composition on crystal chemical comparative analysis, only phosphate members of the shchurovskyite family will be discussed below.

The core of the layers in each structure is a Cu_6 cluster, representing a $[O_2Cu_6]$ dimer of two edge-sharing (OCu_4) tetrahedra, with their bases approximately parallel to the planes of the layers. The dimers form linear rods along *a* in **1**, and along *b* in **2** and other shchurovskyite-type structures, with the shortest Cu···Cu distances between the adjacent dimers varying from 2.866 (in $Rb_2Ca[Cu_3O]_2(PO_4)_4$), to 2.908 and 2.933 (in **2**), and 2.941 Å (in **1**).

Figure 3a shows the projection of the Cu-based layer onto the (010) plane in **1**, with green lines aligned along terminal Cu atoms of dimers of the neighboring rods. The distance between the lines is 2.202 Å. The rods in the structure of **2** are aligned along two-fold screw axis, which results in the different arrangement (Figure 3b). Herein, each rod is surrounded by two symmetrically related rods shifted by 1.654 Å relative to each other. The shift is maximal in the crystal structure of $Rb_2Ca[Cu_3O]_2(PO_4)_4$, where each rod is shifted by 2.820 Å relative to the adjacent rod (Figure 3c).

The results presented above show the highly flexible nature of the shchurovskyite-type structures. Indeed, at least four different structure types are present: triclinic archetype (**1**), monoclinically distorted $1 \times 1 \times 1$ shchurovskyite and its phosphate synthetic analogue with the *C*2 space groups, monoclinically distorted $1 \times 1 \times 2$ superstructure of dmisokolovite with the *C*2/*c* space group, and monoclinically distorted $2 \times 2 \times 2$ superstructure. Both the archetype (**1**) and $2 \times 2 \times 2$ superstructure (**2**) reported herein were obtained in the same experiment, whereas the phosphate analogue of shchurovskyite does not exhibit any significant difference from its parent structure. At the same time, the $1 \times 1 \times 2$ superstructure of dmisokolovite is due to the partial substitution of Cu by Al cations. Thus, the broad variety of shchurovskyite-type structures most likely depends on the flexibility of the Cu-based framework, and the arrangement of the Cu-based rods in particular. We suppose that the flexibility of the Cu-based framework will lead to the discovery of other novel compounds of the series, including novel mineral species.

Another important feature of the shchurovskyite-type structures is the interlayer space that can accommodate different cations, from K^+ (in the structures of dmisokolovite and **2**), to Ca^{2+} (in shchurovskyite and $Rb_2Ca[Cu_3O]_2(PO_4)_4$) and Cu^{2+} (in **1** and **2**). The interlayer sites are responsible for the connection of adjacent Cu-based layers, and it can be assumed that the substitution of non-magnetic cations by Cu^{2+} will lead to significant changes in the magnetic properties of the respective materials.

The differences between the shchurovskyite-related structure types can be easily demonstrated by information-based measures of structural complexity [49–51] (Table 2). In the framework of this approach, the complexity is estimated as the amount of Shannon information contained in a crystal structure according to the following formulas:

$$^{str}I_G = -\sum_{i=1}^{k} p_i \log_2 p_i \quad \text{(bits/atom)} \quad (1)$$

$$^{str}I_G = -v\sum_{i=1}^{k} p_i \log_2 p_i \quad \text{(bits/cell)} \quad (2)$$

where *k* is the number of different crystallographic orbits (independent crystallographic Wyckoff sites) in the structure and p_i is the random choice probability for an atom from the i^{th} crystallographic orbit, which is:

$$p_i = m_i/v \quad (3)$$

where m_i is a multiplicity of a crystallographic orbit (i.e., the number of atoms of a specific Wyckoff site in the reduced unit cell), and v is the total number of atoms in the reduced unit cell.

The crystal structure of **1** (archetype) is the simplest one (3.986 bits/atom and 123.58 bits/cell), whereas the crystal structure of **2** is the most complex in the series (5.974 bits/atom and 1493.446 bits/cell) and belongs to the category of very complex structures [52,53]. The complexity parameters of the crystal structures of shchurovskyite and $Rb_2Ca[Cu_3O]_2(PO_4)_4$ are almost as simple as those for the **1** (4.051 bits/atom and 125.58 bits/cell), whereas the crystal structure of dmisokolovite with the doubled c parameter is twice as complex (4.051 bits/atom and 251.16 bits/cell).

Table 2. Selected crystallographic and structural complexity parameters for shchurovskyite-type structures.

Compound	$K_2Cu[Cu_3O]_2(PO_4)_4$	$K_{2.35}Cu_{0.825}[Cu_3O]_2(PO_4)_4$	$Rb_2Ca[Cu_3O]_2(PO_4)_4$	$K_2Ca[Cu_3O]_2(AsO_4)_4$	$K_3[Cu_5AlO_2](AsO_4)_4$
Space Group	*P*-1	$P2_1/n$	*C*2	*C*2	*C*2/*c*
a, Å	5.779	16.714	16.891	17.286	17.085
b, Å	8.261	11.297	5.641	5.670	5.719
c, Å	8.372	16.803	8.359	8.573	16.533
α, β, γ, °	95.81, 103.24, 96.82	90, 90.77, 90	90, 93.92, 90	90, 92.95, 90	90, 91.72, 90
V, Å^3	382.8	3172.5	794.6	839.2	1614.7
Z	1	8	2	2	4
v, atoms/cell	31	250	31	31	62
I_G, bits/atom	3.986	5.974 *	4.051	4.051	4.051
$I_{G,\,total}$, bits/cell	123.58	1493.446 *	125.58	125.58	251.16
Reference	This work	This work	33	34	34

* All the disordered atoms were placed in their average positions.

Supplementary Materials: The following are available online at https://www.mdpi.com/article/10.3390/cryst11070807/s1, Crystallographic information files of compounds **1** and **2**.

Author Contributions: Conceptualization, I.V.K. and S.V.K.; formal analysis, I.V.K.; investigation, I.V.K.; resources, S.V.K.; writing—original draft preparation, I.V.K.; writing—review and editing, S.V.K.; visualization, I.V.K.; supervision, S.V.K.; project administration, S.V.K.; funding acquisition, S.V.K. All authors have read and agreed to the published version of the manuscript.

Funding: This research was funded by the Russian Science Foundation (grant No. 19-17-00038).

Data Availability Statement: Supplementary crystallographic data for this paper have been deposited at Cambridge Crystallographic Data Centre (CCDC 2092265 and 2092265 for **1** and **2**, respectively) and can be obtained free of charge via www.ccdc.cam.ac.uk/data_request/cif.

Acknowledgments: The XRD measurements were performed at the X-ray Diffraction Centre of St. Petersburg State University.

Conflicts of Interest: The authors declare no conflict of interest.

Appendix A

Table A1. Fractional atomic coordinates and isotropic displacement parameters (Å^2) for **1**.

Atom	x	y	z	U_{eq}
Cu1	0.54313(10)	0.21854(7)	0.18319(7)	0.00826(15)
Cu2	0.62938(11)	0.54189(7)	0.35677(7)	0.01248(16)
Cu3	0.25788(9)	0.51344(7)	0.00581(7)	0.00691(14)
Cu4	1	1	1	0.01075(19)
K1	1.1877(2)	−0.12671(17)	0.39996(14)	0.0251(3)

Table A1. *Cont.*

Atom	x	y	z	U_{eq}
P1	0.5789(2)	−0.14031(14)	0.18292(14)	0.0066(2)
P2	0.9306(2)	0.67348(14)	0.72047(13)	0.0053(2)
O1	0.7258(6)	−0.2413(4)	0.3016(4)	0.0146(7)
O2	0.5839(6)	0.0261(4)	0.2838(4)	0.0102(7)
O3	0.3192(6)	−0.2209(4)	0.1123(4)	0.0134(7)
O4	0.6982(6)	−0.1156(4)	0.0350(4)	0.0106(7)
O5	0.9594(5)	0.5576(4)	0.8563(4)	0.0093(6)
O6	1.1450(5)	0.6696(4)	0.6400(4)	0.0074(6)
O7	0.6911(5)	0.6036(4)	0.5917(4)	0.0093(6)
O8	0.9150(6)	0.8492(4)	0.7897(4)	0.0120(7)
O9	0.5292(5)	0.4366(4)	0.1373(4)	0.0066(6)

Table A2. Fractional atomic coordinates, site occupancy factors (S.O.F.) and isotropic displacement parameters (Å^2) for **1**.

Atom	S.O.F.	x	y	z	U_{eq}
Cu1	1	0.84435(4)	0.42009(6)	0.88948(4)	0.01789(15)
Cu2	1	0.92922(4)	0.41660(6)	0.73252(4)	0.01725(15)
Cu3	1	0.75839(4)	0.54529(5)	0.73128(4)	0.01226(14)
Cu4	1	0.74882(4)	0.30406(5)	0.75677(4)	0.01233(14)
Cu5	1	0.57404(4)	0.39718(6)	0.75159(4)	0.01062(13)
Cu6	1	0.43001(4)	0.59447(7)	0.74471(5)	0.02626(19)
Cu7	1	0.33900(4)	0.56147(6)	0.89307(4)	0.01664(15)
Cu8	1	0.25552(4)	0.44950(5)	0.73520(4)	0.01493(15)
Cu9	1	0.24989(4)	0.69237(5)	0.76032(4)	0.01117(14)
Cu10	1	0.07531(4)	0.59072(5)	0.75522(4)	0.01117(13)
Cu11	1	0.16550(4)	0.58938(6)	0.60214(4)	0.01817(15)
Cu12	1	0.25872(5)	0.82651(7)	0.49436(5)	0.0335(2)
Cu13	1	0.34155(4)	0.58442(6)	0.39884(4)	0.01298(14)
Cu14	0.5	0.10290(9)	0.86289(12)	0.34216(9)	0.0188(3)
Cu15	0.15	0.0595(3)	0.8514(4)	0.3650(3)	0.0188(3)
K1	1	0.23938(9)	0.32812(12)	0.49506(9)	0.0313(3)
K2A	0.41	0.4229(4)	0.8501(4)	0.6448(3)	0.0718(19)
K2B	0.59	0.4599(2)	0.8680(3)	0.5471(3)	0.0613(11)
K3A	0.42	0.4539(10)	0.335(3)	0.5443(9)	0.078(6)
K3B	0.36	0.4585(5)	0.3883(10)	0.5623(9)	0.0382(19)
K3C	0.22	0.445(2)	0.346(4)	0.569(2)	0.069(9)
K4A	0.45	0.5346(3)	0.6385(4)	0.9684(4)	0.0725(17)
K4B	0.55	0.4942(3)	0.7322(5)	1.0182(2)	0.0804(19)
K4C	0.15	0.4597(14)	0.8276(19)	1.042(2)	0.125(12)
K4D	0.55	0.4772(3)	0.9217(6)	1.0477(3)	0.0828(17)
P1	1	0.90143(8)	0.16223(11)	0.83315(8)	0.0099(3)
P2	1	0.90101(7)	0.65707(11)	0.82032(8)	0.0080(2)
P3	1	0.40314(7)	0.33475(11)	0.81544(8)	0.0090(2)
P4	1	0.40152(8)	0.83626(11)	0.83808(8)	0.0111(3)
P5	1	0.34316(8)	0.61861(13)	0.57888(8)	0.0144(3)
P6A	0.337(6)	0.3350(19)	1.0893(18)	0.5736(18)	0.011(3)
P6B	0.663(6)	0.3349(9)	1.0612(9)	0.5739(10)	0.0129(17)
P7	1	0.16036(8)	1.05119(12)	0.42170(8)	0.0130(3)
P8	1	0.16418(8)	0.62317(12)	0.41864(8)	0.0125(3)
O1	1	0.9538(2)	0.1157(4)	0.7643(3)	0.0240(10)
O2	1	0.8989(3)	0.0726(4)	0.9004(3)	0.0289(11)
O3	1	0.9302(2)	0.2838(3)	0.8587(2)	0.0173(8)

Table A2. *Cont.*

Atom	S.O.F.	*x*	*y*	*z*	U_{eq}
O4	1	0.8155(2)	0.1732(3)	0.7957(2)	0.0161(8)
O5	1	0.9596(2)	0.5784(3)	0.7737(2)	0.0141(8)
O6	1	0.8775(3)	0.5963(3)	0.8971(2)	0.0192(9)
O7	1	0.8277(2)	0.6751(3)	0.7635(2)	0.0152(8)
O8	1	0.9385(2)	0.7797(3)	0.8364(2)	0.0105(7)
O9	1	0.4379(2)	0.2116(3)	0.8333(2)	0.0162(8)
O10	1	0.3249(2)	0.3197(3)	0.7645(2)	0.0167(8)
O11	1	0.4600(2)	0.4076(3)	0.7625(2)	0.0165(8)
O12	1	0.3874(3)	0.3991(3)	0.8928(2)	0.0194(8)
O13	1	0.4321(2)	0.7117(3)	0.8570(3)	0.0210(9)
O14	1	0.4578(2)	0.9000(4)	0.7807(3)	0.0239(10)
O15	1	0.3901(3)	0.9127(4)	0.9113(3)	0.0320(11)
O16	1	0.3197(2)	0.8238(3)	0.7932(2)	0.0159(8)
O17	1	0.3869(2)	0.6187(4)	0.5003(2)	0.0272(10)
O18A	0.337(6)	0.3132(7)	0.7541(10)	0.5773(7)	0.0199(12)
O18B	0.663(6)	0.2644(4)	0.6911(5)	0.5798(4)	0.0199(12)
O19A	0.337(6)	0.4069(9)	0.6053(15)	0.6410(9)	0.021(3)
O19B	0.663(6)	0.4004(4)	0.6670(8)	0.6433(5)	0.0221(17)
O20A	0.337(6)	0.2739(8)	0.5379(11)	0.5834(8)	0.0258(13)
O20B	0.663(6)	0.3189(4)	0.4881(6)	0.5983(4)	0.0258(13)
O21	1	0.4024(3)	1.0565(5)	0.6340(3)	0.0390(13)
O22A	0.337(6)	0.2806(18)	0.9835(18)	0.5575(14)	0.044(6)
O22B	0.663(6)	0.3011(7)	0.9367(8)	0.5635(7)	0.030(2)
O23	1	0.2682(3)	1.1526(5)	0.6017(3)	0.0374(12)
O24	1	0.3724(3)	1.1141(5)	0.4974(3)	0.0325(11)
O25	1	0.1884(3)	0.9209(4)	0.4246(3)	0.0269(10)
O26	1	0.2261(2)	1.1350(4)	0.3955(2)	0.0189(8)
O27	1	0.0901(2)	1.0434(4)	0.3599(2)	0.0271(10)
O28	1	0.1255(3)	1.0924(4)	0.5000(2)	0.0209(9)
O29	1	0.1786(3)	0.4971(3)	0.3940(2)	0.0228(9)
O30	1	0.1071(2)	0.6862(4)	0.3573(2)	0.0199(9)
O31	1	0.2454(2)	0.6921(3)	0.4201(2)	0.0147(8)
O32	1	0.1241(2)	0.6348(4)	0.5000(2)	0.0191(8)
O33	1	0.8264(2)	0.4268(3)	0.7770(2)	0.0094(7)
O34	1	0.6801(2)	0.4241(3)	0.7134(2)	0.0092(7)
O35	1	0.3253(2)	0.5669(3)	0.7799(2)	0.0110(7)
O36	1	0.1812(2)	0.5730(3)	0.7141(2)	0.0116(7)

References

1. Han, T.-H.; Singleton, J.; Schlueter, J.A. Barlowite: A spin-1212 antiferromagnet with a geometrically perfect kagome motif. *Phys. Rev. Lett.* **2014**, *113*, 227203. [CrossRef]
2. Norman, M.R. Herbertsmithite and the search for the quantum spin liquid. *Rev. Mod. Phys.* **2016**, *88*, 041002. [CrossRef]
3. Zheng, X.G.; Kawae, T.; Kashitani, Y.; Li, C.S.; Tateiwa, N.; Takeda, K.; Yamada, H.; Xu, C.N.; Ren, Y. Unconventional magnetic transitions in the mineral clinoatacamite $Cu_2Cl(OH)_3$. *Phys. Rev. B Condens. Matter Mater. Phys.* **2005**, *71*, 052409. [CrossRef]
4. Zheng, X.G.; Mori, T.; Nishiyama, K.; Higemoto, W.; Yamada, H.; Nishikubo, K.; Xu, C.N. Antiferromagnetic transitions in polymorphous minerals of the natural cuprates atacamite and botallackite $Cu_2Cl(OH)_3$. *Phys. Rev. B Condens. Matter Mater. Phys.* **2005**, *71*, 174404. [CrossRef]
5. Li, Y.-S.; Zhang, Q.-M. Structure and magnetism of S = 1/2 kagome antiferromagnets $NiCu_3(OH)_6Cl_2$ and $CoCu_3(OH)_6Cl_2$. *J. Phys. Condens. Matter.* **2013**, *25*, 026003. [CrossRef]
6. Malcherek, T.; Mihailova, B.; Welch, M.D. Structural phase transitions of clinoatacamite and the dynamic Jahn-Teller effect. *Phys. Chem. Miner.* **2017**, *44*, 307–321. [CrossRef]
7. Malcherek, T.; Welch, M.D.; Williams, P.A. The atacamite family of minerals—A testbed for quantum spin liquids. *Acta Crystallogr.* **2018**, *B74*, 519–526. [CrossRef]
8. Vilminot, S.; André, G.; Richard-Plouet, M.; Bourée-Vigneron, F.; Kurmoo, M. Magnetic Structure and Magnetic Properties of Synthetic Lindgrenite, $Cu_3(OH)_2(MoO_4)_2$. *Inorg. Chem.* **2006**, *45*, 10938–10946. [CrossRef] [PubMed]
9. Belik, A.A.; Koo, H.-J.; Whangbo, M.-H.; Tsujii, N.; Naumov, P.; Takayama-Muromachi, E. Magnetic Properties of Synthetic Libethenite Cu_2PO_4OH: A New Spin-Gap System. *Inorg. Chem.* **2007**, *46*, 8684–8689. [CrossRef] [PubMed]

10. Janson, O.; Tsirlin, A.A.; Schmitt, M.; Rosner, H. Large quantum fluctuations in the strongly coupled spin-1/2 chains of green dioptase $Cu_6Si_6O_{18}·6H_2O$. *Phys. Rev. B Condens. Matter Mater. Phys.* **2010**, *82*, 014424. [CrossRef]
11. Podlesnyak, A.; Prokhorenko, O.; Nikitin, S.E.; Kolesnikov, A.I.; Matsuda, M.; Dissanayake, S.E.; Prisk, T.R.; Nojiri, H.; Díaz-Ortega, I.F.; Kidder, M.K.; et al. magnetic ground state and magnetic excitations in black dioptase $Cu_6Si_6O_{18}$. *Phys. Rev. B Condens. Matter Mater. Phys.* **2019**, *100*, 184401. [CrossRef]
12. Hiroi, Z.; Ishikawa, H.; Yoshida, H.; Yamaura, J.-I.; Okamoto, Y. Orbital Transitions and Frustrated Magnetism in the Kagome-Type Copper Mineral Volborthite. *Inorg. Chem.* **2019**, *58*, 11949–11960. [CrossRef] [PubMed]
13. Yoshida, H.; Michiue, Y.; Takayama-Muromachi, E.; Isobe, M. β-Vesignieite $BaCu_3V_2O_8(OH)_2$: A structurally perfect $S = 1/2$ kagomé antiferromaget. *J. Matter. Chem.* **2012**, *22*, 18793–18796. [CrossRef]
14. Boldrin, D.; Knight, K.; Wills, A.S. Orbital frustration in the $S = 1/2$ kagome magnet vesignieite, $BaCu_3V_2O_8(OH)_2$. *J. Matter. Chem. C* **2016**, *4*, 10315–10322. [CrossRef]
15. Sun, W.; Huang, Y.-X.; Pan, Y.; Mi, J.-X. Synthesis and magnetic properties of centennialite: A new $S = 1/2$ Kagomé antiferromagnet and comparison with herbertsmithite and kapellasite. *Phys. Chem. Miner.* **2016**, *43*, 127–136. [CrossRef]
16. Vilminot, S.; Richard-Plouet, M.; André, G.; Swierczynski, D.; Guillot, M.; Bourée-Vigneron, F.; Drillon, M.; André, G.; Swierczynski, D.; Guillot, M.; et al. Magnetic structure and properties of $Cu_3(OH)_4SO_4$ made of triple chains of spins $s = 1/2$. *J. Solid State Chem.* **2003**, *170*, 255–264. [CrossRef]
17. Brandão, P.; Rocha, J.; Reis, M.S.; dos Santos, A.M.; Jin, R. Magnetic properties of $KNaMSi_4O_{10}$ compounds (M = Mn, Fe, Cu). *J. Solid State Chem.* **2009**, *182*, 253–258. [CrossRef]
18. Jahn, H.A.; Teller, E. Stability of polyatomic molecules in degenerate electronic states. *Proc. R. Soc. Ser. A* **1937**, *161*, 220–235.
19. Hathaway, B.J. A new look at the stereochemistry and electronic properties of complexes of the copper(II) ion. In *Complex Chemistry. Structure and Bonding*; Emsley, J., Ernst, R.D., Hathaway, B.J., Warren, K.D., Eds.; Springer: Berlin/Heidelberg, Germany, 1984; Volume 57, pp. 55–118.
20. Burns, P.C.; Hawthorne, F.C. Static and dynamic Jahn-Teller effects in Cu^{2+} oxysalt minerals. *Can. Mineral.* **1996**, *34*, 1089–1105.
21. Effenberger, H. Contribution to the Stereochemistry of Copper. The Transition from a Tetragonal Pyramidal to a Trigonal Bipyramidal Cu(II)O_5 Coordination Figure with a Structure Determination of $PbCu_2(SeO_3)_3$. *J. Solid State Chem.* **1988**, *73*, 118–126. [CrossRef]
22. Eby, R.K.; Hawthorne, F.C. Structural Relations in Copper Oxysalt Minerals. I. Structural Hierarchy. *Acta Crystallogr. Sect. B Struct. Sci. Cryst. Eng. Mater.* **1993**, *49*, 28–56. [CrossRef]
23. Burns, P.C.; Hawthorne, F.C. Coordination-geometry structural pathways in Cu^{2+} oxysalt minerals. *Can. Mineral.* **1995**, *33*, 889–905.
24. Krivovichev, S.V.; Filatov, S.K. Structural principles for minerals and inorganic compounds containing anion-centered tetrahedra. *Am. Mineral.* **1999**, *84*, 1099–1106. [CrossRef]
25. Krivivochev, S.V.; Mentré, O.; Siidra, O.I.; Colmont, M.; Filatov, S.K. Anion-Centered Tetrahedra in Inorganic Compounds. *Chem. Rev.* **2013**, *113*, 6459–6535. [CrossRef]
26. Volkova, L.M.; Marinin, D.V. Frustrated Antiferromagnetic Spin Chains of Edge-Sharing Tetrahedra in Volcanic Minerals $K_3Cu_3(Fe_{0.82}Al_{0.18})O_2(SO_4)_4$ and $K_4Cu_4O_2(SO_4)_4$MeCl. *J. Supercond. Nov. Magn.* **2017**, *30*, 959–971. [CrossRef]
27. Badrtdinov, D.I.; Kuznetsova, E.S.; Verchenko, V.Y.; Berdonosov, P.S.; Dolgikh, V.A.; Mazurenko, V.V.; Tsirlin, A.A. magnetism of coupled spin tetrahedra in ilinskite-type $KCu_5O_2(SeO_3)_2Cl_3$. *Sci. Rep.* **2018**, *8*, 2379. [CrossRef]
28. Botana, A.S.; Zheng, H.; Lapidus, S.H.; Mitchell, J.F.; Norman, M.R. Averievite: A copper oxide kagome antiferromagnet. *Phys. Rev. B* **2018**, *98*, 054421. [CrossRef]
29. Winiarski, M.J.; Tran, T.T.; Chamorro, J.R.; McQueen, T.M. (CsX)$Cu_5O_2(PO_4)_2$ (X = Cl, Br, I): A Family of Cu^{2+} $S = \frac{1}{2}$ Compounds with Capped-Kagomé Networks Composed of OCu_4 Units. *Inorg. Chem.* **2019**, *58*, 4328–4336. [CrossRef]
30. Siidra, O.I.; Vladimirova, V.A.; Tsirlin, A.A.; Chukanov, N.V.; Ugolkov, V.L. $Cu_9O_2(VO_4)_4Cl_2$, the first copper oxychloride vanadate: Mineralogically inspired synthesis and magnetic behavior. *Inorg. Chem.* **2020**, *59*, 2136–2143. [CrossRef] [PubMed]
31. Fujihala, M.; Morita, K.; Mole, R.; Mitsuda, S.; Tohyama, T.; Yano, S.-I.; Yu, D.; Sota, S.; Kuwai, T.; Koda, A.; et al. Gapless spin liquid in a square-kagome lattice antiferromagnet. *Nat. Commun.* **2020**, *11*, 3429. [CrossRef]
32. Kornyakov, I.V.; Vladimirova, V.A.; Siidra, O.I.; Krivovichev, S.V. Expanding the Averievite Family, (MX)$Cu_5O_2(T^{5+}O_4)_2$ (T^{5+} = P, V; M = K, Rb, Cs, Cu; X = Cl, Br): Synthesis and Single-Crystal X-ray Diffraction Study. *Molecules* **2021**, *26*, 1833. [CrossRef]
33. Aksenov, S.M.; Borovikova, E.Y.; Mironov, V.S.; Yamnova, N.A.; Volkov, A.S.; Ksenofontov, D.A.; Gurbanova, O.A.; Dimitrova, O.V.; Deyneko, D.V.; Zvereva, E.A.; et al. $Rb_2CaCu_6(PO_4)_4O_2$, a novel oxophosphate, with a shchurovskyite-type topology: Synthesis, structure, magnetic properties and crystal chemistry of rubidium copper phosphate. *Acta Crystallogr.* **2019**, *B75*, 903–913. [CrossRef]
34. Pekov, I.V.; Zubkova, N.V.; Belakovskiy, D.I.; Yapaskurt, V.O.; Vigasina, M.F.; Sidorov, E.G.; Pushcharovsky, D.Y. New arsenate minerals from the Arsenatnaya fumarole, Tolbachik volcano, Kamchatka, Russia. IV. Shchurovskyite, $K_2CaCu_6O_2(AsO_4)_4$ and dmisokolovite, $K_3Cu_5AlO_2(AsO_4)_4$. *Mineral. Mag.* **2015**, *79*, 1737–1753. [CrossRef]
35. Kornyakov, I.V.; Krivovichev, S.V.; Gurzhiy, V.V. Oxocentered Units in Three Novel Rb-Containing Copper Compounds Prepared by CVT Reactions Method. *Z. Anorg. Allg. Chem.* **2018**, *644*, 77–81. [CrossRef]
36. Kovrugin, V.M.; Siidra, O.I.; Colmont, M.; Mentré, O.; Krivovichev, S.V. Emulating exhalative chemistry: Synthesis and structural characterization of ilinskite, $Na[Cu_5O_2](SeO_3)_2Cl_3$, and its K-analogue. *Miner. Petrol.* **2015**, *109*, 421–430. [CrossRef]

37. Jing, B.; Peng, C.; Wang, Y.; Liu, Q.; Tong, S.; Zhang, Y.; Ge, M. Hygroscopic properties of potassium chloride and its internal mixtures with organic compounds relevant to biomass burning aerosol particles. *Sci. Rep.* **2015**, *7*, 43572. [CrossRef]
38. Giamarelou, M.; Smith, M.; Papapanagiotou, E.; Martin, S.; Biskos, G. Hygroscopic properties of potassium-halide nanoparticles. *Aerosol Sci. Technol.* **2018**, *52*, 536–545. [CrossRef]
39. Brunel-Laügt, M.; Guitel, J.-C. Structure crystalline de $Cu_5O_2(PO_4)_2$. *Acta Crystallogr.* **1977**, *B33*, 3465–3468. [CrossRef]
40. *CrysAlisPro Software System*, version 1.171.38.46; Rigaku Oxford Diffraction: Oxford, UK, 2015.
41. Sheldrick, G.M. SHELXT—Integrated space-group and crystal structure determination. *Acta Crystallogr.* **2015**, *A71*, 3–8. [CrossRef]
42. Sheldrick, G.M. Crystal structure refinement with SHELXL. *Acta Crystallogr.* **2015**, *C71*, 3–8.
43. Dolomanov, O.V.; Bourhis, L.J.; Gildea, R.J.; Howard, J.A.K.; Puschmann, H. OLEX2: A complete structure solution, refinement and analysis program. *J. Appl. Cryst.* **2009**, *42*, 339–341. [CrossRef]
44. Pekov, I.V.; Zubkova, N.V.; Agakhanov, A.A.; Pushcharovsky, D.Y.; Yapaskurt, V.O.; Belakovskiy, D.I.; Vigasina, M.F.; Sidrov, E.G.; Britvin, S.N. Cryptochalcite, $K_2Cu_5O(SO_4)_5$, and cesiodymite, $CsKCu_5O(SO_4)_5$, two new isotypic minerals and the K-Cs isomorphism in this solid-solution series. *Eur. J. Mineral.* **2018**, *30*, 593–607. [CrossRef]
45. Siidra, O.I.; Lukina, E.A.; Nazarchuk, E.V.; Depmeier, W.; Bubnova, R.S.; Agakhanov, A.A.; Avdontseva, E.Y.; Filatov, S.K.; Kovrugin, V.M. Saranchinaite, $Na_2Cu(SO_4)_2$, a new exhalative mineral from Tolbachik volcano, Kamchatka, Russia, and a product of the reversible dehydration of kröhnkite, $Na_2Cu(SO_4)_2(H_2O)_2$. *Mineral. Mag.* **2018**, *82*, 257–274. [CrossRef]
46. Berry, R.S. Correlation of Rates of Intramolecular Tunneling Processes, with Application to Some Group V Compounds. *J. Chem. Phys.* **1960**, *32*, 933–938. [CrossRef]
47. Pasquarello, A.; Petri, I.; Salmon, P.S.; Parisel, O.; Car, R.; Tóth, E.; Powell, D.H.; Fischer, H.E.; Helm, L.; Merbach, A.E. First Solvation Shell of the Cu(II) Aqua Ion: Evidence for Fivefold Coordination. *Science* **2001**, *291*, 856–859. [CrossRef]
48. McCusker, L.B.; Liebau, F.; Engelhardt, G. Nomenclature of structural and compositional characteristics of ordered microporous and mesoporous materials with inorganic hosts: (IUPAC recommendations 2001). *Microporous Mesoporous Mater.* **2003**, *58*, 3–13. [CrossRef]
49. Krivovichev, S.V. Topological complexity of crystal structures: Quantitative approach. *Acta Crystallogr.* **2012**, *A68*, 393–398. [CrossRef] [PubMed]
50. Krivovichev, S.V. Structural complexity of minerals: Information storage and processing in the mineral world. *Miner. Mag.* **2013**, *77*, 275–326. [CrossRef]
51. Krivovichev, S.V. Structural complexity and configurational entropy of crystalline solids. *Acta Crystallogr.* **2016**, *B72*, 274–276.
52. Krivovichev, S.V. Ladders of information: What contributes to the structural complexity in inorganic crystal. *Z. Kristallogr.* **2018**, *233*, 155–161. [CrossRef]
53. Krivovichev, S.V. Which inorganic structures are the most complex? *Angew. Chem. Int. Ed.* **2014**, *53*, 654–661. [CrossRef] [PubMed]